PERGAMON

International Journal of Multiphase Flow 28 (2002) 731–755

International Journal of Multiphase Flow

www.elsevier.com/locate/ijmulflow

Instantaneous hydrodynamics of a laminar wavy liquid film

K. Moran, J. Inumaru [1], M. Kawaji *

Department of Chemical Engineering and Applied Chemistry, University of Toronto, 200 College Street, Toronto, Ont., Canada, M5S 3E5

Received 28 June 1999; received in revised form 19 December 2001

Abstract

Experiments have been conducted to investigate instantaneous hydrodynamic characteristics of laminar falling films of 20 cS silicone oil on an inclined plate using a photochromic dye activation technique and high-speed video photography over a Reynolds number range of 11–220. Instantaneous velocity profiles across a wavy laminar film and axial profiles of film thickness have been measured simultaneously and statistically analyzed. Experimental data indicated that the time-averaged mean and maximum velocity data are significantly over-predicted by Nusselt's theory, while the time-averaged film thickness data are slightly under-predicted. The instantaneous velocity profiles examined in different regions of the wavy laminar film showed that in the smooth substrate film region, the velocity profiles matched Nusselt theory, however, under the large waves they were substantially smaller than Nusselt's predictions for films of the same thickness. Based on the measured velocity profiles, approximately 30–40% of liquid mass was estimated to be transported by the large waves. The instantaneous wall shear stress values were close to the gravity force per unit area in the substrate film, but much smaller under the large waves. The temporal variations of wall shear stress and film thickness showed that the peaks in wall shear stress more often preceded the film thickness peaks, suggesting that the liquid in the wave region experiences acceleration, while in the non-wavy region both acceleration and deceleration are experienced. © 2002 Published by Elsevier Science Ltd.

Keywords: Laminar falling film; Wavy film; Hydrodynamics; Nusselt's theory; Photochromic dye activation; Velocity profile

* Corresponding author. Tel.: +1-416-978-3063; fax: +1-416-978-8605.
E-mail address: kawaji@ecf.toronto.edu (M. Kawaji).
[1] Central Research Institute of Electric Power Industry, Yokosuka, Japan.

0301-9322/02/$ - see front matter
PII: S0301-9322(02)00006-X

1. Introduction

Liquid films on vertical or inclined surfaces falling under the influence of gravity are important in many industrial applications, including wetted-wall absorbers, condensers, vertical tube evaporators, and falling film chemical reactors. In order to design these types of industrial equipment reliably the transport rates of heat and mass must be accurately predicted. However, the interfacial and wall-to-liquid heat and mass transport processes for wavy falling films are significantly affected by the unsteady hydrodynamic characteristics of the wavy films such as the film thickness, velocity distribution, and wall shear stress variations, which are not yet fully understood over a wide range of Reynolds numbers.

Nusselt (1916) analyzed falling liquid films theoretically, assuming a steady rectilinear flow with a flat, smooth and shear-free gas–liquid interface. He arrived at the following equations describing the parabolic velocity profile, $u(y)$, wall shear stress, τ_w, and thickness, δ, of a laminar liquid film of density, ρ, and viscosity, μ, flowing downward on a plate inclined at an angle, θ, from the vertical:

$$u(y) = \frac{\rho g \delta^2 \cos\theta}{2\mu}\left[\frac{2y}{\delta} - \left(\frac{y}{\delta}\right)^2\right] \tag{1}$$

$$\tau_w = \rho g \delta \cos\theta \tag{2}$$

$$\delta = \left[3\mu U_m / \rho g \cos\theta\right]^{0.5} \tag{3}$$

where g is the acceleration due to gravity and U_m is the mean film velocity.

Experimentally, the hydrodynamic characteristics of falling liquid films have been investigated vigorously in the past, however, the small and fluctuating thickness of these films, often observed to be in the order of millimeters, has presented considerable difficulties to the measurements of local flow structures. Many film thickness measurements have been conducted in the past to better understand the film characteristics such as the variation of mean or time-averaged film thickness with Reynolds number, axial variation of mean film thickness, temporal variations in local film thickness and statistical nature of interfacial waves.

Various techniques have also been used to measure velocities in falling liquid films including an ultramicroscope technique, stereoscopic photography, volumetric hold-up and laser Doppler anemometry, among others. Most of the previous investigations of velocity and velocity profiles, however, yielded time-averaged data. Grimley (1945) reported significant deviations of the measured velocity profiles in wavy water films from the parabolic profile predicted by Nusselt (1916). However, Wilkes and Nedderman (1962), Cook and Clark (1971), and Mudawar and Houpt (1993b) all reported good agreement with a parabolic distribution for water and highly viscous falling films. In the latter study, a large degree of fluctuation from a parabolic distribution was also observed.

Instantaneous velocity profiles are more difficult to measure experimentally in falling liquid films, mainly due to their small and fluctuating thickness. Nakoryakov et al. (1977) used stroboscopic visualization of spherical aluminum particles in water–glycerin films to measure the velocity profiles together with a shadow graph method to determine the instantaneous film thickness. Alekseenko et al. (1985) extended the above study and reported that at $Re = 50$ the velocity profiles under interfacial waves are well behaved and conform to a self-similar parabolic

profile, with little fluctuations. In regions of extended substrate the velocity profiles were reported to agree well with the parabolic velocity profile predicted by Nusselt (1916). The most interesting results, however, were that in regions immediately surrounding waves the fluctuations in velocity profile were very large, and a significantly smaller velocity profile than Nusselt's profile corresponding to the same film thickness was seen for several waves.

Ho and Hummel (1970) used the photochromic dye activation technique to measure velocity profiles in vertical, annular falling films of aqueous alcohol solutions and alcohol–glycerol mixtures in which the formation of waves was suppressed by addition of a surface-active agent, over a Reynolds number range of 124–2800. This technique involves the reversible activation of a photochromic dye dissolved in the working fluid, and has been applied to various two-phase flow studies recently (Kawaji et al., 1993; Kawaji, 1998).

The wall shear stress in falling liquid films has been measured by Brauer (1956) for film flow on the exterior of a vertical tube, and by Fulford (1964) for falling films in an inclined channel. The time-averaged wall shear stress values for the smooth laminar regime conformed to the classical prediction of Nusselt (1916), however, in the wavy laminar region, Fulford (1964) indicated the wall shear stress was greater than the classical prediction. Using an electrochemical technique, Wasden and Dukler (1989) measured the wall shear stress in vertical annular falling films of aqueous solutions at a Reynolds number of 880, and reported that the wall shear stress achieved peak values in the wave-front region, as opposed to the wave crest. Lyu and Mudawar (1991) and Brauner and Moalem-Maron (1982) also reported similar trends for freely falling, laminar wavy water films. Aragaki et al. (1990) also used the electrochemical technique in a vertical, annular falling film, and their results for $100 < Re < 600$ indicated good agreement with the wall shear stress values calculated from Nusselt's theory (Eqs. (2) and (3)).

On the theoretical side, much progress has been made on the analysis of wave evolution in laminar film flow (for example, see a review by Chang et al. (1993)), and considerable efforts have been spent on the theoretical understanding of falling liquid films (e.g., Shkadov, 1967; Alekseenko et al., 1994). Numerical simulations of wavy laminar falling films have also been conducted (Brauner and Moalem-Maron, 1983; Moalem-Maron et al., 1989; Wasden and Dukler, 1989; Nagasaki and Hijikata, 1989; Yu et al., 1995; Stuhltrager et al., 1995; among others) to simultaneously predict the temporal and spatial variations in film thickness, wall shear stress and/or velocity fields. Jayanti and Hewitt (1997) also solved an energy equation to predict heat transfer rates under solitary waves. However, to our knowledge, velocity field predictions for wavy films have not been compared with instantaneous flow field data to a sufficient extent, since such experimental data are extremely scarce.

Thus, the purpose of the present work was to obtain instantaneous film thickness, velocity profile and wall shear stress data simultaneously in a viscous liquid film flowing down an inclined, smooth plate in a rectangular channel over a sufficiently wide range of Reynolds numbers. High-speed video photography and the photochromic dye activation technique were used to directly measure the instantaneous axial profiles of wavy liquid film thickness and stream-wise velocity profiles. The relationships among fluctuating film thickness, instantaneous velocity profiles and wall shear stress have been examined.

A second dimensionless parameter that has been identified to be important for characterizing laminar falling films besides Reynolds number is Kapitza number, $\gamma = \sigma/\rho v^{4/3} g^{1/3}$, where σ is surface tension and v is kinematic viscosity (Shkadov and Sisoev, 1999; Chang, 1994). In this

work, only the Reynolds number was varied for a single fluid, and the effects of Kapitza number on the wavy film characteristics were assessed by comparisons with other experimental and numerical results in the literature reported for different Kapitza numbers.

2. Experimental apparatus and method

The flow loop was designed to enable the delivery of fully developed, gravity driven liquid flow in the test section under constant pressure head (Fig. 1). The test section consisted of a smooth, polished copper plate, 80 mm wide (W) and 1.92 m long (L), inclined at an angle of 45° from the vertical ($\theta = 45°$), and equipped with transparent polycarbonate side walls to enable viewing of the longitudinal cross-section of the liquid film. The total length of the test section, including the upper plenum, was 2.27 m and the entrance to the copper plate was smoothly rounded to ensure evenly distributed flow across the entire width of the channel.

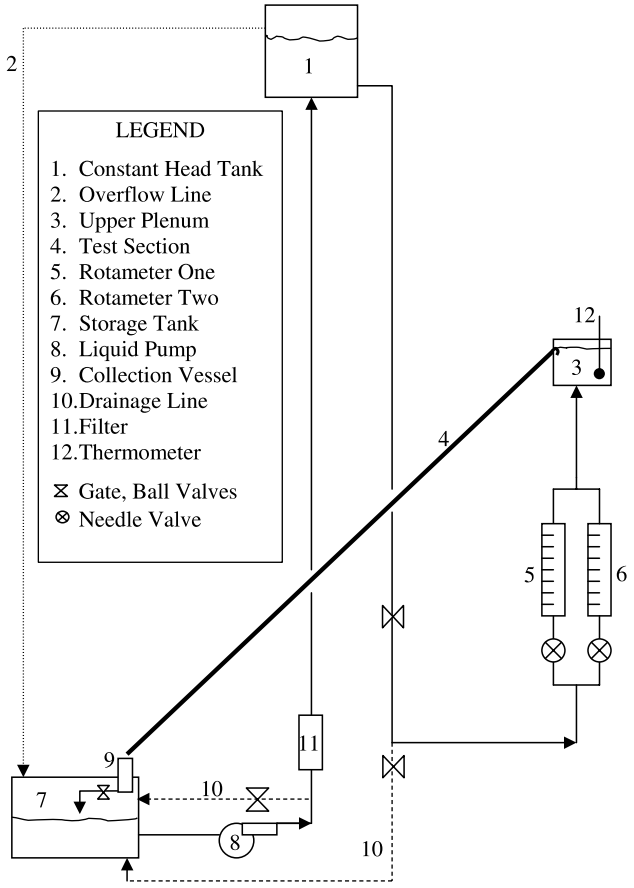

Fig. 1. Experimental flow loop.

The liquid flow rate was monitored and controlled by means of two flow meters located in the flow loop upstream of the upper plenum, up to the maximum flow rate of 6.2 LPM. The upper plenum was designed to reduce the liquid velocity and allow a smooth entry into the test section. The liquid was then collected from the end of the test section in a lucite collection vessel.

The working fluid used in this study was Silicone Fluid 200, manufactured by Dow Corning. Its physical properties at a temperature of 22 °C are as follows: kinematic viscosity, $\nu = 2 \times 10^{-5}$ m^2/s (or 20 cS), density, $\rho = 960$ kg/m^3, and surface tension, $\sigma = 2.06 \times 10^{-2}$ N/m. With these property values, the Kapitza number, γ, is equal to 18.4. The photochromic dye used was 1′,3′,3′-trimethylindoline-2-spiro-2-benzospyran (TNSB), which provided an instantaneous and reversible photochromic reaction upon exposure to UV light. The TNSB dye was dissolved in the silicone fluid to a maximum concentration of 0.015% by weight, which had a negligible effect on surface tension due to the low concentration used and the fact that the dye molecules remain homogeneously dispersed throughout the entire liquid.

In the photochromic dye activation technique, pulses of a UV laser beam at 335 nm wavelength from a nitrogen gas laser (Photonics PRA UV-24) were directed at the liquid film to create photochromic dye traces at the plane of symmetry (40 mm from the side walls) and 1.3 m from the test section inlet. The laser beam was directed normal to the liquid film surface to create dark purple traces across the film. To focus the beam and enhance the formation of a well-defined, thin trace, an optical lens with a focal length of 25 cm was placed at the aperture of the laser. A high intensity sodium lamp (General Electric Lucalox, model LU1000) operating at 1000 W, with an AC high frequency inverter, provided the back lighting.

The dye traces formed by the laser pulses were captured with a high-speed CCD video camera (Photron HVC 11B) at a rate of 186 frames per second. A 35 mm lens was used in conjunction with a 20 mm extension ring to obtain a view field size of approximately 6.40 mm (height) by 7.44 mm (width). The UV pulse laser was operated at a frequency of 50–60 Hz at high *Re* and at 20–30 Hz at lower *Re*, to produce successive dye traces across the film. The video images provided both the instantaneous trace data as well as the axial profile of the liquid film thickness. For each run, 60 instantaneous velocity profiles and film thickness data were obtained at equally spaced time intervals to compute time-averaged parameters over the sampling period of 2.8 s.

Experiments were run at a temperature of 22 ± 0.5 °C and at 11 different volumetric flow rates, Q, covering a Reynolds number range of 11–220. Various measurement uncertainties in the data were estimated and are given below as a percentage of the value reported, except for the liquid flow rate.

Film thickness	5.3–2.1%	from low to high *Re*
Wall shear stress	23–4.6%	from low to high *Re*
Average velocity	18–2.5%	from low to high *Re*
Instantaneous velocity	18–1.7%	from low to high *Re*
Maximum velocity	13–1.7%	from low to high *Re*
Liquid flow rate	±0.02 LPM	for $11 < Re < 26$
	±0.3 LPM	for $69 < Re < 220$

The wall shear stress and velocity errors were obtained by a propagation of error analysis. More details of the experimental apparatus, procedure and measurement technique can be found in Moran (1997).

3. Results and discussion

The development of the wave structure could be observed by following the liquid as it flowed through the test section. The liquid film exhibited a smooth, flat gas–liquid interface upon immediate entrance to the test section, but after a short distance small, two-dimensional ripples were observed at the interface. These ripples then proliferated into a defined wavy structure with large fronts and elongated tails. At approximately 60 cm from the inlet, the two-dimensional waves developed into a three-dimensional structure characterized by large waves. In between these larger wave structures, smaller waves of saw-toothed shape could be observed. In general, the degree of waviness increased with increasing Reynolds number. Dukler and Bergelin (1952) reported a similar increase in the waviness of a water film ($\gamma \sim 3000$) as the Reynolds number was increased from 482 to 2770. Consecutive video images of typical dye traces of the falling liquid film at $Re = 122$ depict the location of the trace relative to the bounding wall and the gas–liquid interface (Fig. 2).

3.1. Time-averaged hydrodynamic parameters

The time-averaged film thickness, mean and maximum velocities, and wall shear stress data obtained in each run are summarized in Table 1. The second column of Table 1 shows the liquid flow rate, Q, obtained from the flow meter readings. The mean film thickness, δ, was evaluated by averaging 60 instantaneous film thickness data. The mean velocity, U_{ave}, and maximum velocity, U_{max}, were obtained by time-averaging the instantaneous mean velocity, $U_{m,i}$, and the maximum velocity evaluated at the interface ($y = \delta$), respectively. The instantaneous mean velocity, $U_{m,i}$, was computed by integrating each instantaneous velocity profile, $u(y)$, across the film thickness, δ_i.

The Reynolds number, $Re = 4U_{ave}\delta/v$, shown in Table 1 is based on the measured mean velocity and mean film thickness. The wall shear stress, τ_w, was evaluated by time-averaging the instantaneous wall shear stress which was obtained from instantaneous velocity gradient (du/dy) at the wall ($y = 0$) multiplied by liquid viscosity. The second last column lists the time-averaged gravitational force per unit area, $\rho g \delta \cos\theta$, based on the measured mean film thickness, which represents Nusselt's (1916) prediction of wall shear stress for a steady, smooth film flow. The last

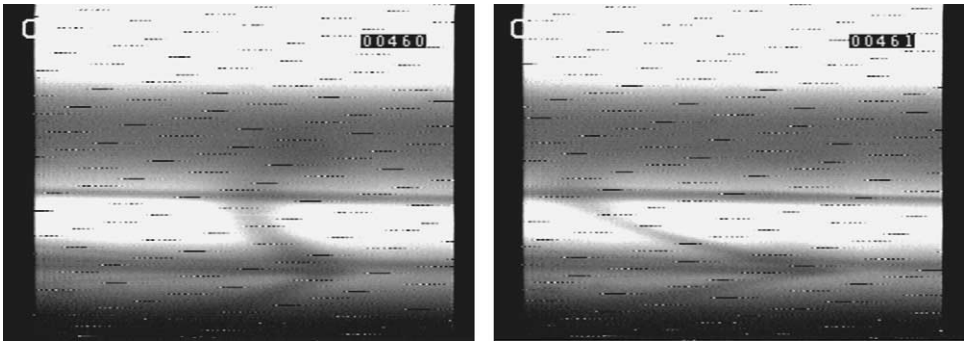

Fig. 2. Typical sequential recordings of a trace profile in a liquid film at $Re = 122$.

Table 1
Summary of time-averaged flow characteristics

Run no.	Q (LPM)	δ (mm)	U_{ave} (m/s)	U_{max} (m/s)	Re	τ_w (Pa)	$\rho g \delta \cos\theta$ (Pa)	Wave frequency (Hz)
1.6	0.333	0.91	0.063	0.089	11	6.31	6.09	1
1.10	0.333	0.91	0.070	0.099	13	6.25	6.07	1.5
2.1	0.405	0.92	0.076	0.109	15	6.42	6.15	1.8
2.2	0.405	0.92	0.079	0.116	15	6.41	6.12	2.2
3.2	0.476	0.99	0.087	0.127	18	6.48	6.56	3.3
4.1	0.548	1.04	0.091	0.133	20	6.98	6.92	2.2
4.3	0.548	1.04	0.091	0.143	21	7.19	6.89	2.8
5.3	0.619	1.09	0.103	0.149	24	7.06	7.22	3.3
5.4	0.619	1.07	0.110	0.162	26	7.56	7.14	2.8
52.1	1.72	1.48	0.218	0.320	71	10.3	9.86	4
52.2	1.72	1.56	0.206	0.313	69	10.9	10.4	4
62.1	2.55	1.73	0.279	0.404	107	12.0	11.5	4
62.2	2.55	1.72	0.249	0.383	95	12.3	11.4	4.3
72.1	3.25	1.81	0.311	0.467	122	12.4	12.0	4.3
82.1	4.02	1.93	0.365	0.539	150	13.4	12.8	5.5
82.3	4.02	2.08	0.351	0.539	156	13.6	13.8	5
92.1	4.78	2.09	0.419	0.621	189	14.5	13.5	5.3
92.2	4.40	2.17	0.376	0.575	175	14.2	14.5	6
10.1	5.15	2.13	0.440	0.662	202	14.4	14.2	6.5
10.3	5.45	2.31	0.449	0.682	220	14.5	15.4	7

column of Table 1 shows the frequency of large-amplitude waves, which are simply referred to as waves hereafter. After extensively viewing the axial film thickness profiles recorded by the high-speed video camera, the wave was defined in this paper as a region that has a film thickness greater than 1.15 times the mean film thickness for each run. Since at least one trace was formed in each wave, the number of waves included in each data set was equal to at least the sampling period (2.8 s) times the wave frequency.

In order to verify the accuracy of the instantaneous film thickness and velocity profile measurements, the average liquid flow rate, Q_{ave}, calculated from the measured velocity profiles was compared with the actual volumetric flow rate, Q, from the rotameter readings shown in Table 1. The calculated flow rate, Q_{ave}, was obtained for each run by time averaging the product of the instantaneous mean velocity, instantaneous film thickness and channel width, assuming the same flow characteristics existed uniformly across the channel width. A comparison of the calculated flow rates, Q_{ave}, with the actual flow rates, Q, showed reasonably good agreement between them, mostly within the measurement uncertainties of ± 0.3 LPM for high flow rates ($69 < Re < 220$), and ± 0.02 LPM for low flow rates ($11 < Re < 26$).

3.1.1. Film thickness

The mean film thickness was calculated by averaging 60 instantaneous film thickness data, δ_i, for each of the 20 runs analyzed,

$$\overline{\delta} = \frac{\sum_{i=1}^{N} \delta_i}{N} \tag{4}$$

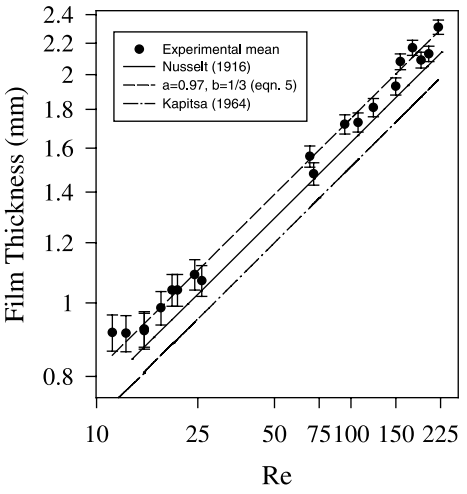

Fig. 3. Variation of mean film thickness with Reynolds number.

The mean film thickness increases with the Reynolds number as shown in Fig. 3 which follows the general trend first proposed by Nusselt (1916) for a smooth laminar film. This film thickness relation may be restated as,

$$\delta = a(v^2/g\cos\theta)^{1/3}Re^b \tag{5}$$

where a and b are constants. Nusselt (1916) theory predicts the constants to be $a = 0.909$ and $b = 1/3$ for the present silicone fluid film flowing over a flat plate with a 45° inclination. The present mean film thickness data could also be fitted by Eq. (5) with similar constants of $a = 0.97$ and $b = 1/3$, and the measured film thickness was slightly under-predicted by Nusselt's (1916) theory by 6.7%. Although this difference appears to be small, the effect of film thickness discrepancy on the film flow rate prediction can be quite large because the liquid velocity is the largest in the interface region. Kapitza's (1965) theoretical model, attempting to account for the effects of regular periodic waves and surface tension in a falling laminar film, is seen to under-predict both the present film thickness data and Nusselt's (1916) model.

Although some authors have reported that the time-averaged film thickness of wavy films is over-predicted by Nusselt's equation (e.g., Kapitza, 1965; Portalski, 1963), others have obtained results similar to ours. Takahama and Kato's (1980) mean film thickness data for laminar water films ($\gamma \sim 3000$, $Re = 200$–400) were 5% larger than Nusselt's theory. Karapantsios et al. (1989) also found that Nusselt's (1916) theory under-predicts their mean thickness data for a wavy water film although the Reynolds number range tested was slightly higher than that of this study.

3.1.2. Mean and maximum velocities

In Fig. 4, the time-averaged mean and maximum velocities are plotted against the measured mean film thickness and also compared with Nusselt's (1916) equation,

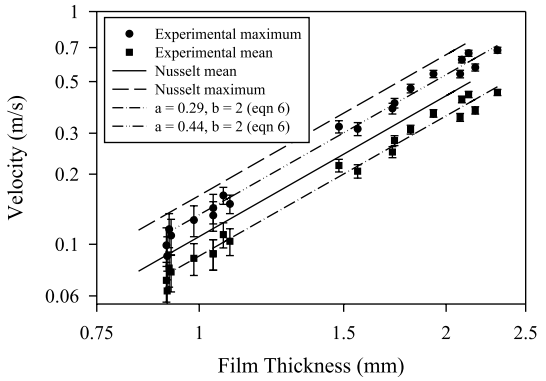

Fig. 4. Comparison of mean and maximum velocities with Nusselt's theory.

$$U = a(g\cos\theta/\nu)\delta^2 \tag{6}$$

where $a = 1/3$ for the mean velocity and 1/2 for the maximum velocity. The present data can also be correlated by Eq. (6) with $a = 0.29$ for the mean velocity and 0.44 for the maximum velocity, but the data show constant negative deviations from Nusselt (1916) predictions for both the mean and maximum velocities. If the measured mean film thickness is used as in Fig. 4, Nusselt's equation is seen to over-predict both the mean and maximum velocity data, on the average, by 12.9% and 13.6%, respectively. This over-prediction of the mean velocity resulted from the use of the measured film thickness in Eq. (6), which was greater than that predicted for a given Reynolds number as shown in Fig. 3.

According to Nusselt's (1916) parabolic velocity profile, the ratio of maximum-to-mean velocity in the laminar film is given by,

$$\frac{U_{\max}}{U_{\mathrm{m}}} = \frac{3}{2} \tag{7}$$

The time-averaged maximum-to-mean velocity ratios obtained experimentally fell between 1.42 and 1.56, with an overall average of 1.47, slightly lower than Nusselt's (1916) prediction. Therefore, the time-averaged velocity profiles obtained in this study are generally parabolic in nature as previously suggested for laminar falling films. However, the instantaneous velocity profiles in wavy films can deviate significantly from Nusselt's (1916) profile as will be discussed in greater detail in the subsequent sections.

The present time-averaged maximum-to-mean velocity ratio of 1.47 is slightly higher than the value of 1.4 obtained by Portalski (1964) at $Re = 600$ for a falling film of water–glycerin solution with a Kapitza number, $\gamma \sim 1$. On the other hand, Koziol et al. (1981) obtained values of $U_{\max}/U_{\mathrm{ave}} \sim 1.8$ at $Re = 500$–700, for a water film ($\gamma \sim 3000$) falling on an inclined plate, significantly greater than the present value. Thus, the maximum-to-mean velocity ratio appears to increase with the Kapitza number, however, it is difficult to draw a reliable conclusion on the Kapitza number dependence due to an insufficient amount of data available for comparable ranges of Reynolds numbers.

3.1.3. Wall shear stress

The time-averaged wall shear stress values, τ_w, calculated from the velocity gradients measured at the wall agree well with Nusselt's (1916) predictions, $\rho g \delta \cos\theta$, for a smooth, laminar film, which exhibits a linear dependence on the mean film thickness (Table 1). The largest positive deviation of 4.6% from Nusselt's (1916) theory occurred at lower Reynolds numbers, while the largest negative deviation of 6.2% occurred at higher Reynolds numbers. These deviations from Nusselt's (1916) theory may be again due to the effects of the waves as discussed in the next section.

3.2. Instantaneous flow variables

It was shown above that the time-averaged hydrodynamic characteristics for a wavy, laminar falling film can be predicted with some deviations by the steady state equations of Nusselt (1916). To better understand these deviations, it would be useful to examine the local, instantaneous values and temporal fluctuations of these parameters. Fig. 5 shows the local fluctuations of film thickness, flow rate, velocity (local mean and maximum), and wall shear stress at $Re = 122$. The dashed lines indicate the time-averaged values, and the results shown are typical of all data collected. All experimental runs were carefully examined in the above manner in order to compare

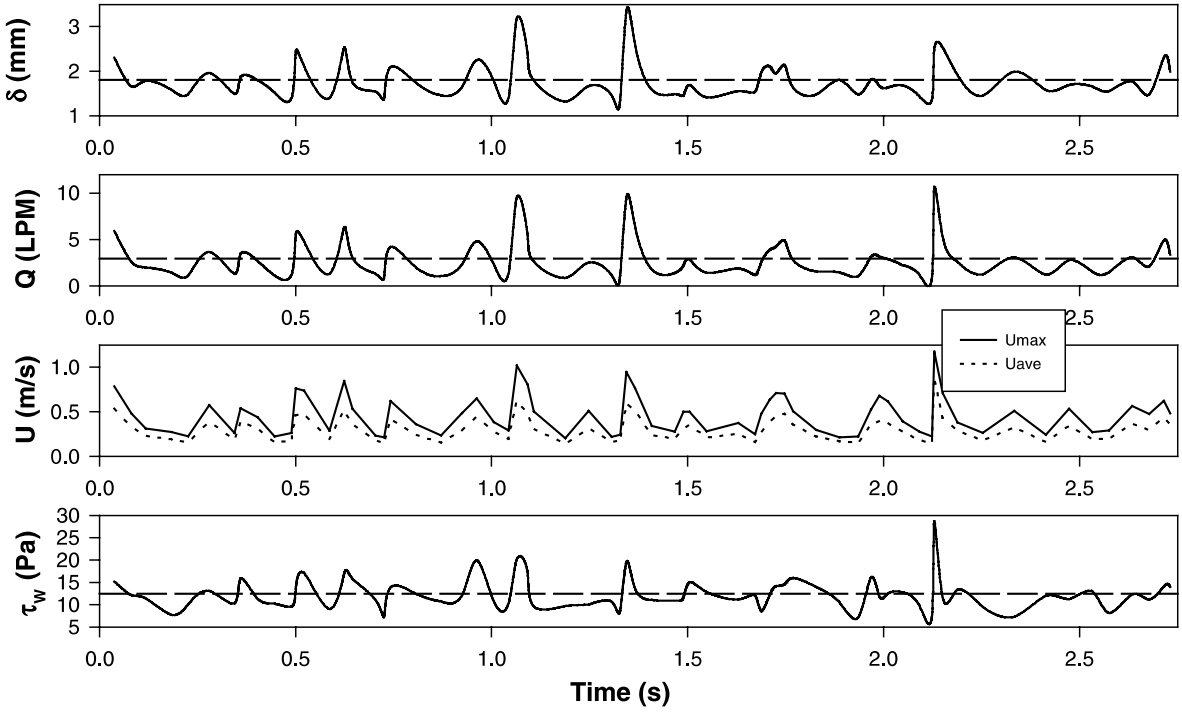

Fig. 5. Instantaneous hydrodynamic characteristics at $Re = 122$.

the variations in instantaneous film thickness with the other hydrodynamic parameters mentioned.

Generally, the film thickness was always found to decrease dramatically before a large wave, and this decrease was less for smaller waves. All the hydrodynamic parameters were found to significantly fluctuate about the time-averaged values, and the amplitude of fluctuations increased with the Reynolds number. The instantaneous volumetric flow rate, average velocity and maximum velocity appeared to follow the local fluctuations in film thickness quite closely. It did not, however, appear that the variations followed any constant proportional relationship with the film thickness. The instantaneous wall shear stress exhibited a lesser tendency (relative to other parameters) to follow the variations in the local film thickness. In low Re flows, the wall shear stress appeared to fluctuate around the time-averaged mean value in extended regions of a substrate layer.

A more detailed analysis of many of the instantaneous hydrodynamic parameters mentioned above is presented below.

3.2.1. Waves and substrate film thickness

The wavy laminar film consists of smooth substrate film and large wave regions (Dukler, 1977). There are small waves with short wavelengths preceding the large amplitude waves which have much greater wavelengths. Chu and Dukler (1975) defined the substrate thickness based on a statistical approach by evaluating the probability density function (p.d.f.) of the instantaneous film thickness data. In the present work, the p.d.f. of instantaneous film thickness was evaluated at 0.1 mm intervals to study the film waviness at different Reynolds numbers, as shown in Fig. 6. At low Reynolds numbers ($Re = 13$ and 24), the p.d.f. distributions showed a sharp peak at about 1.0 mm, but remained close to zero for greater thickness values, indicating existence of few waves. As the Reynolds number increased to 106 and 220, additional smaller peaks appeared to the right of the main peaks at about 1.3 and 1.8 mm, respectively. The main peak indicates the most probable film thickness, which can be considered to represent the substrate film thickness, and the additional peaks at greater film thickness values correspond to the small and large amplitude waves. In the present experiment, the substrate film thickness remained relatively constant at 0.85–0.95 mm for $Re = 11$–26, but increased with Reynolds number for $69 < Re < 220$. As expected, the substrate film thickness remained below the mean film thickness shown in Fig. 3 earlier.

The root-mean-square (RMS) values of the film thickness fluctuations and maximum film thickness, both normalized by Nusselt's mean film thickness, δ_N, are plotted against Re in Fig. 7. At low Reynolds numbers ($11 < Re < 26$), the RMS values increased rapidly with Re but then gradually decreased with Re for $69 < Re < 220$. The values of $\delta_{RMS}/\delta_N = 0.25$–0.32 at $Re = 200$–220 for the present film with $\gamma = 18.4$, are similar to the values reported for water with $\gamma = 3550$ at $Re = 200$ (Yu et al., 1995). The normalized maximum film thickness also increased rapidly at low Reynolds numbers, but then remained relatively constant at a value of about 2.2 for $69 < Re < 220$. For falling films of aqueous solutions ($\gamma \sim 3500$), Wasden and Dukler (1992) reported a normalized maximum wave amplitude of about 2 at $Re = 230$. Chu and Dukler (1975) presented maximum wave amplitude-to-mean film thickness ratios of about 3.0 for a falling film of water ($\gamma \sim 3000$) at $Re = 570$. Comparisons of present data with others available suggest a relatively small effect of Kapitza number on the normalized liquid film fluctuation amplitude and maximum film thickness.

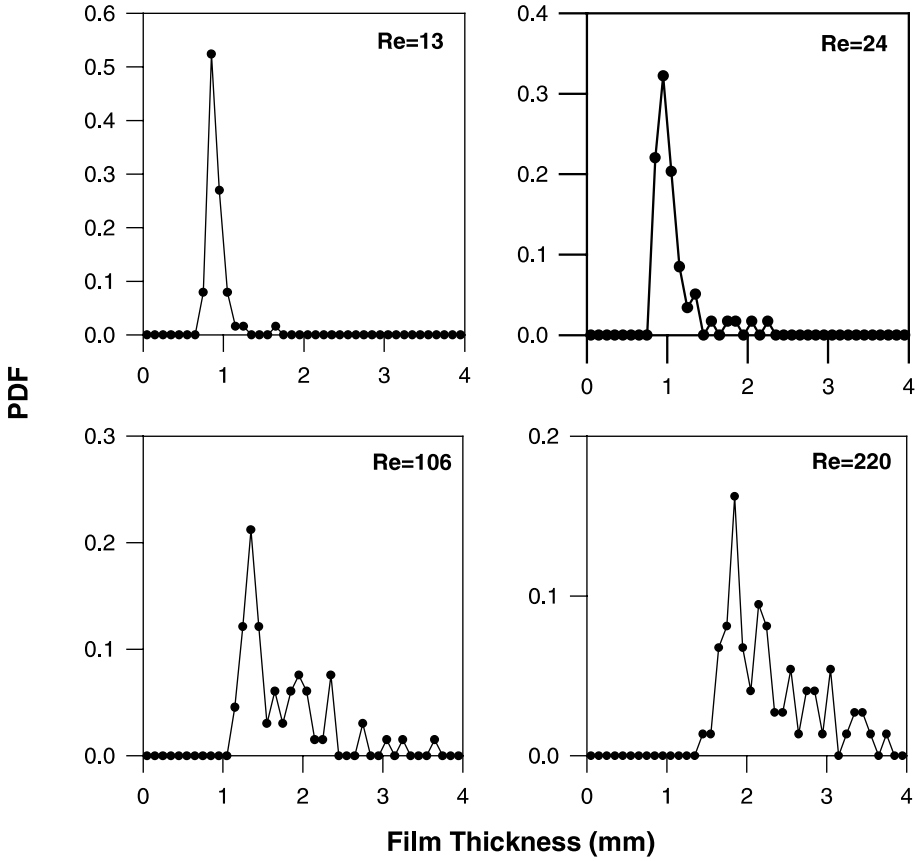

Fig. 6. P.d.f.s of local film thickness at different Reynolds numbers.

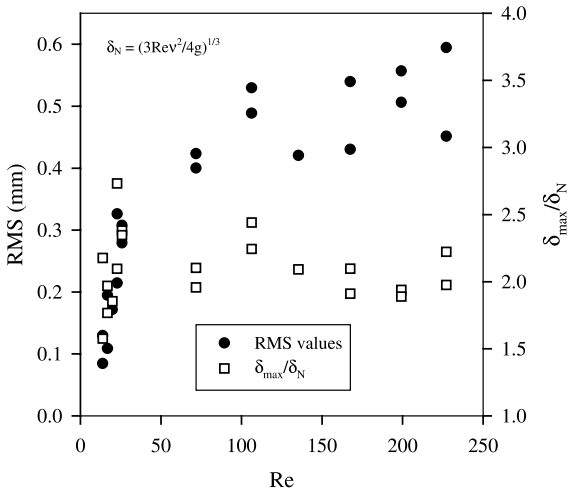

Fig. 7. Variations of RMS of film thickness fluctuations and maximum film thickness with Reynolds number.

The wave frequency was determined from the film thickness history data, such as those shown in Fig. 5, by counting the number of waves with a thickness greater than 1.15 times the mean film thickness. It was also checked by comparing with the frequency of waves observed on the video recordings. As shown in Table 1, the wave frequency was found to increase with the Reynolds number from 1 to 3 Hz for $Re = 11$–26 to 4–7 Hz for $Re = 69$–220.

3.2.2. Instantaneous velocity profiles

The local, instantaneous velocity profiles were calculated for all runs and approximately $n = 60$–80 profiles were obtained in each run. Typical plots are presented in Fig. 8, where all the velocity profiles obtained are shown for the designated run. Different vertical scales are used for these plots in order to effectively examine each set of profiles.

Some interesting observations can be made based on careful examinations of the measured velocity profiles, such as those shown in Fig. 8.

(a) The velocity profiles in the wavy film can be divided into two groups belonging to the substrate film and the waves. The substrate film region, evident by the relatively small maximum distance from the wall, was associated with velocity profiles that achieved relatively

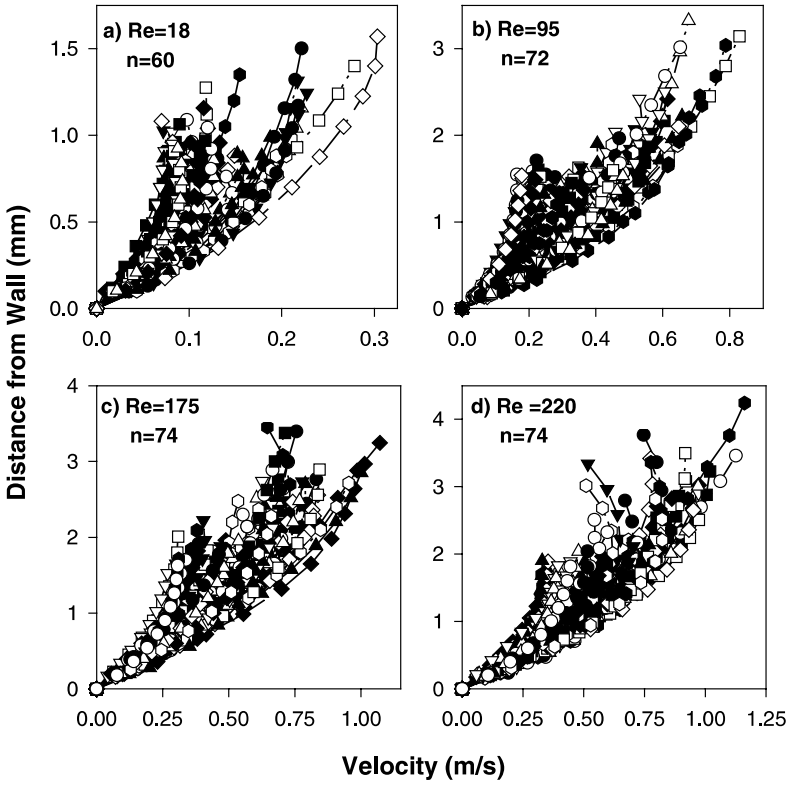

Fig. 8. Instantaneous velocity profiles at different Reynolds numbers.

low maximum velocities and appear on the left side of each plot. The wavy regions of the falling film gave resultant velocity profiles characterized by relatively large maximum velocities appearing on the right side of each plot in Fig. 8.

(b) At low Reynolds numbers, although relatively few waves were present as seen by the small number of velocity profiles covering large distances from the wall with high velocities, the instantaneous velocity profiles showed large fluctuations in the substrate region. This is consistent with Alekseenko et al.'s (1985) observation for a vertically falling film of a water–glycerin solution ($\gamma \sim 200$) at a Reynolds number of 50. In other words, the substrate film surrounding a wave structure was strongly influenced by the presence of the large-amplitude waves.

(c) As the Reynolds number increased, the occurrence of thick film regions (presumably waves) also became more frequent, as evident from the appearance of more high velocity data at large distances from the wall. Consequently, the degree of velocity profile fluctuations increased in both the substrate film and wavy regions. Above a Reynolds number of 69, the boundary between the substrate and wavy regions was no longer distinct, and the maximum velocity did not always occur at the gas–liquid interface, especially in the wavy region.

(d) The photochromic dye traces did not yield any direct evidence of circulatory motion under the waves with peak-to-substrate ratios less than about 2.5 in the present range of low Reynolds numbers tested. This is consistent with the numerical simulation results of Moalem-Maron et al. (1989), Yu et al. (1995), and Jayanti and Hewitt (1997) for $Re < 600$, in which vortex motions were predicted only for waves of a water film ($\gamma \sim 3000$) with wave amplitude/substrate thickness ratios greater than a critical value of about 2.5. Although the Kapitza number is quite different, the absence of vortex motions under the wave crests for low Reynolds numbers and wave peak-to-substrate thickness ratios less than 2.5 is consistent between the present experiment and above simulation results.

It is evident that the waves play a significant role in the hydrodynamics of falling films on an inclined plate, including their obvious effect on the instantaneous velocity profiles. Individual velocity profiles are further examined to elucidate the effects of waves on the hydrodynamics of laminar falling films. In Fig. 9, the instantaneous velocity profiles normalized by the maximum instantaneous velocity, $U_{\max,i}$, are plotted against the distance from the wall scaled by the instantaneous liquid film thickness, δ_i, to determine whether or not the instantaneous profiles are self-similar and always conform to Nusselt's profile indicated by a solid curve with circles. The normalized velocity profiles generally follow Nusselt's profile at all Reynolds numbers covered, however, significant deviations can be observed for some instantaneous profiles with peaks occurring well below the liquid film surface.

To study the deviations more carefully, a series of figures are presented depicting small time-wise portions (on the order of 0.45 s) of the film thickness fluctuations and the associated velocity profiles (Figs. 10 and 11). The instantaneous velocity profiles are seen to be generally parabolic and fluctuate around Nusselt's (1916) prediction in most regions except under the wave crests as mentioned above. The velocity profiles under the waves are clearly over-predicted by Nusselt's theory. Careful examinations of these figures and similar data from other runs, revealed the following:

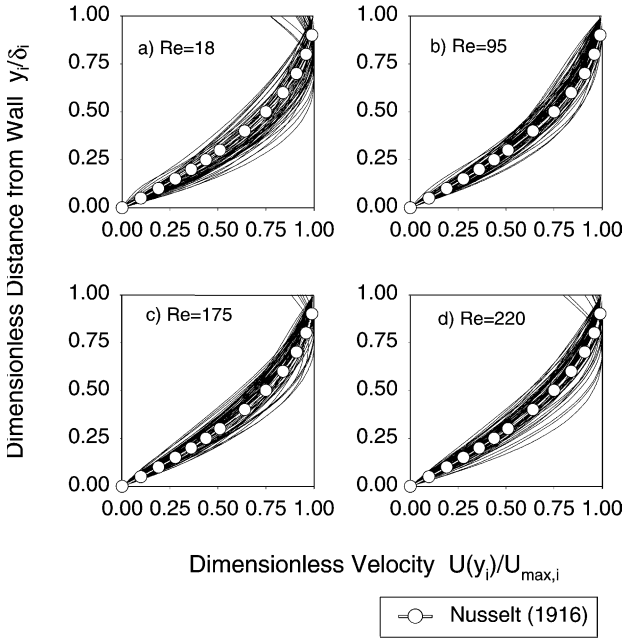

Fig. 9. Instantaneous velocity profiles normalized by the maximum velocity.

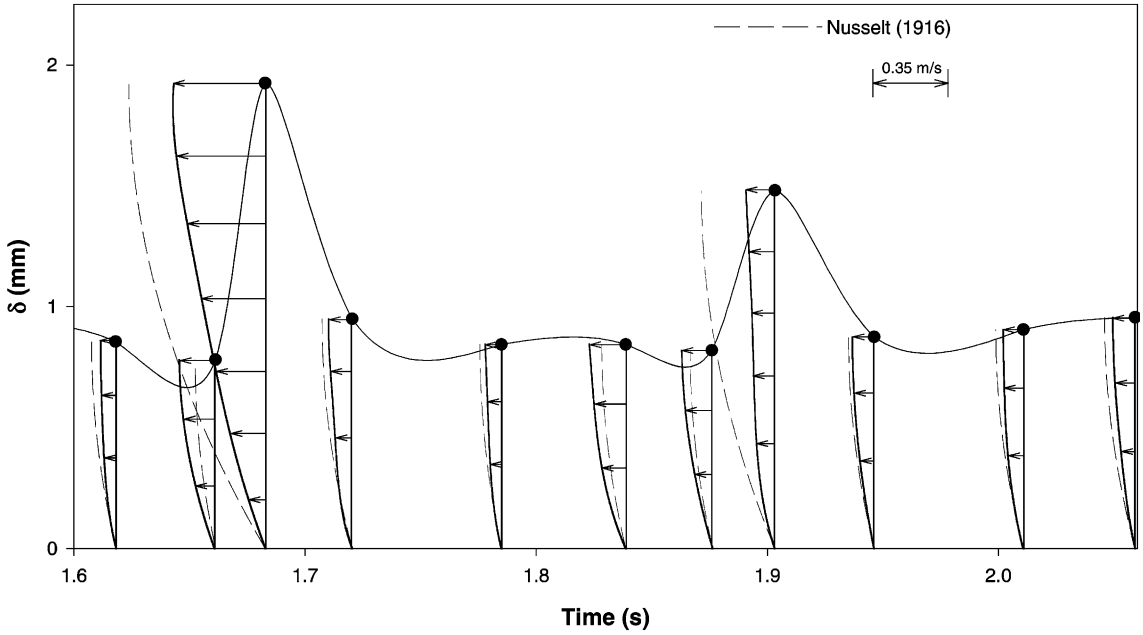

Fig. 10. Variations of instantaneous velocity profile and film thickness at $Re = 26$.

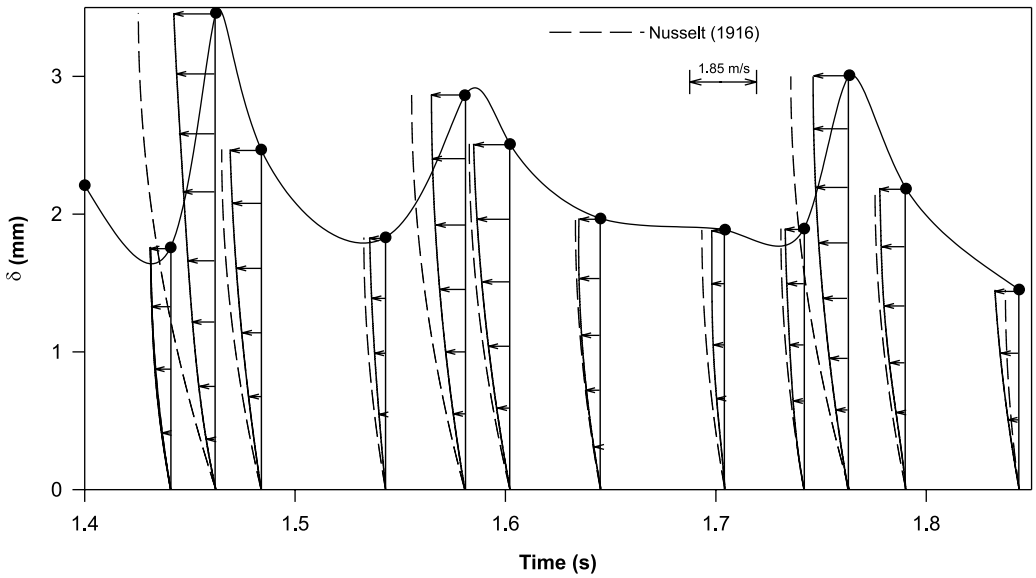

Fig. 11. Variations of instantaneous velocity profile and film thickness at $Re = 220$.

(a) The instantaneous velocity profiles in the smooth film region followed Nusselt's (1916) prediction quite closely, with less than 10% deviations. This is consistent with a limited amount of velocity profile data reported by Alekseenko et al. (1985) for the substrate region of a vertical water–glycerin film ($\gamma \sim 200$) at $Re = 50$, which showed good agreement with Nusselt's (1916) profile. Numerical simulations of a wavy R-11 condensate ($\gamma = 2671$) film falling on a vertical wall by Stuhltrager et al. (1995) also showed an identical velocity profile in the substrate film as Nusselt's profile at $Re = 350$.

(b) Significant over-predictions of velocity profiles by Nusselt's (1916) theory were always observed under the large wave crests, with deviations of the order of 100% in many instances. These severe deviations would account for some of the over-predictions of time-averaged mean and maximum velocities (Fig. 4). This result is again consistent with the measurements of Alekseenko et al. (1985), which showed that the velocity profiles under large waves compare very well with a self-similar parabolic profile, but are about half as large as Nusselt's (1916) profile for the same film thickness. Numerical predictions by Stuhltrager et al. (1995) for a falling film of R-11 ($\gamma = 2671$) also showed a significantly smaller velocity profile under the crest of a large wave with a peak-to-substrate film thickness ratio of about 2. At $Re = 350$, the velocity profile under the wave crest was predicted to be nearly parabolic but the surface velocity was about 30% less than that given by Nusselt's (1916) profile for the same film thickness. Although the present data are for a liquid film flowing down a 45° inclined plate, they are consistent with the vertical falling film results described above.

(c) In regions immediately preceding and following the wave crest (i.e., wave-front and wave-back regions, respectively), the velocity profiles were observed to be in better agreement with Nusselt's (1916) theory than under the wave crests, but still over-predicted by Nusselt's (1916) theory by as much as 30%. Alekseenko et al. (1994) also reported the instantaneous

Table 2
Statistical analysis of mean velocity profiles in different regions of wavy films

Region	Detection criteria	No. of samples averaged	Deviation from Nusselt's mean velocity (%)	$\tau_w/\rho g\delta\cos\theta$
Wave	$\delta_{i-1} < \delta_i > \delta_{i+1}$ and $\delta_i > 1.15\delta_{ave}$	181	−44.3	0.93
Wave-back	$\delta_{i-1} > \delta_i > \delta_{i+1}$ and $\delta_{i-1} > 1.15\delta_{ave}$	211	−23.0	1.03
Wave-front	$\delta_{i-1} < \delta_i < \delta_{i+1}$ or $\delta_{i-1} > \delta_i < \delta_{i+1}$ and $\delta_{i+1} > 1.15\delta_{ave}$	200	−6.8	1.06
Substrate	$\delta_i < 0.9\delta_{ave}$	357	−5.1	1.08

velocity profiles in the wave-front and wave-back regions of a water-glycerin film ($\gamma = 200$) at $Re = 50$ to be under-developed and also deviate from the parabolic velocity profile by 15%. On the other hand, Stuhltrager et al. (1995) numerically predicted a greater velocity profile than Nusselt's profile in the wave-back region,but close agreement between the two in the wave-front region. This difference between the present data and Stuhltrager et al.'s (1995) numerical results for the wave-back region may be due to the shape of the wavy film profile predicted and the parts of the film considered as the wave front and wave back.

In order to analyze the deviations of instantaneous velocity profiles from Nusselt's predictions in different parts of the wavy film more quantitatively, the instantaneous velocity profile data were statistically analyzed in the following manner. First, the wave, wave-front, wave-back and substrate film regions were identified from the consecutive film thickness data such as those shown in Figs. 10 and 11 as follows. Each film thickness data, δ_i, was examined along with the previous and next film thickness, δ_{i-1} and δ_{i+1}, respectively, to be classified into one of four regions based on the criteria shown in Table 2.

Although some data did not fit any of the criteria and were left out of the analysis, sufficiently large numbers of film thickness and velocity profile data were obtained in each region as shown in the third column. In all four regions, the instantaneous mean velocity obtained by averaging each velocity profile across the film was found to be less than the mean velocity given by Nusselt's equation for a smooth film of the same thickness, as shown in the second last column of Table 2. The standard deviations were such that in the wave and wave-back regions, the instantaneous mean velocities were always less than Nusselt's values, while they fluctuated about Nusselt's value in the substrate film.

3.2.3. Maximum-to-mean velocity ratio

The instantaneous values of maximum-to-mean velocity ratio are shown in Fig. 12 for six Reynolds numbers. The ratios as high as 2.0 were obtained although the average value over the whole *Re* range studied was 1.47 ± 0.04 as mentioned previously. The instantaneous maximum-to-mean velocity ratio was found to fluctuate around this mean value for all Reynolds numbers but the amplitude of fluctuations did not change appreciably over the Reynolds number range examined. Although the falling film studied in this work was laminar, the waves caused considerable variations in the local velocity profiles even close to the wall as evident in Fig. 8. In the

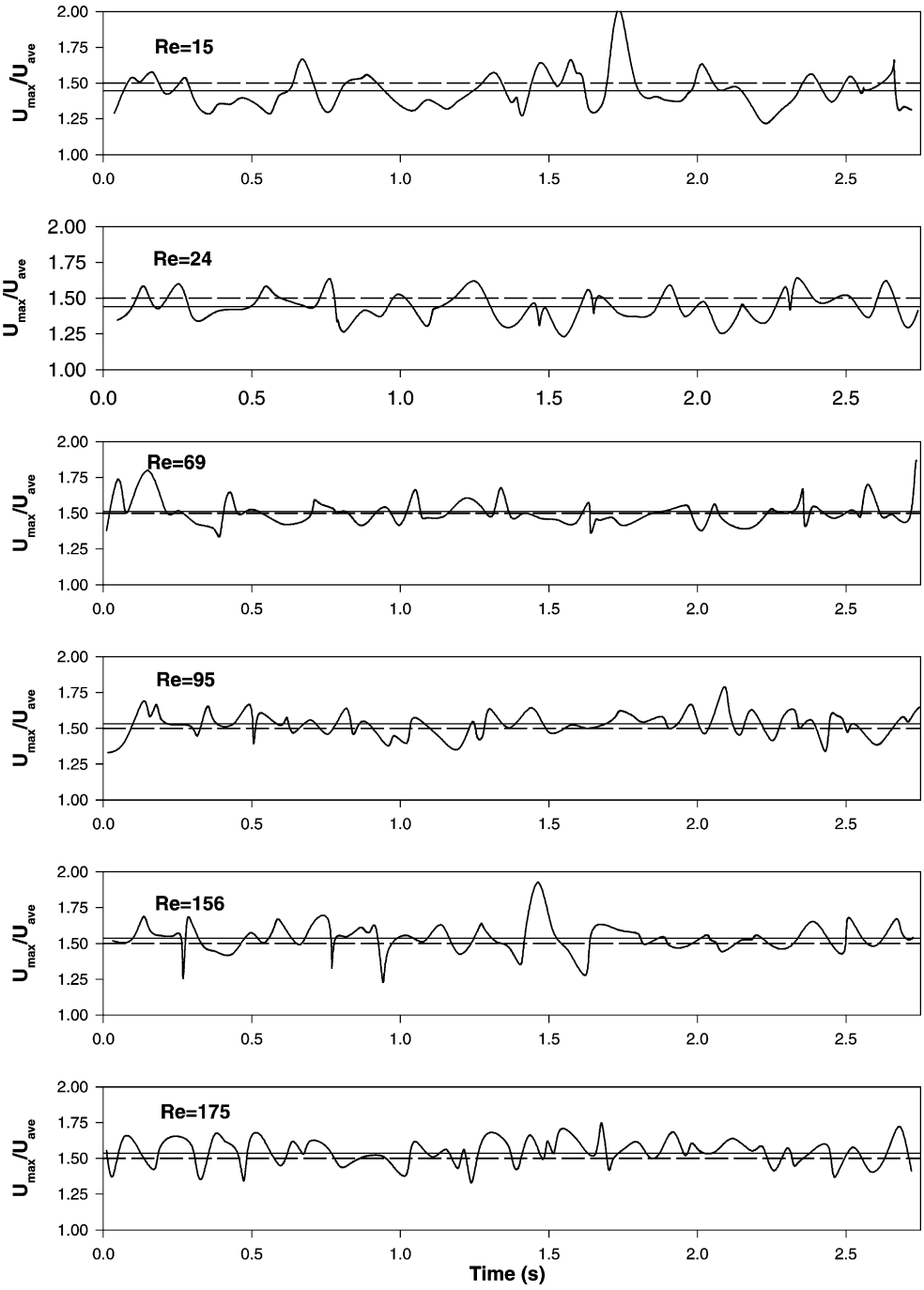

Fig. 12. Instantaneous fluctuations of maximum-to-mean velocity ratio. (---Eq. (7); solid straight line: time average value).

wave front, the higher velocity liquid under the wave could exert some influence on the preceding substrate, possibly causing acceleration of the liquid in this region. Similarly, in the wave-back

region the presence of a wave, decelerating by this point, may also accelerate the liquid in the substrate following the wave.

3.2.4. Liquid mass transported by waves

In the past, an increase in heat and mass transfer across the interface in wavy falling films has been attributed to the effects of large-amplitude waves and small waves that cover the large waves and substrate film. The large waves are believed to contain surface renewing eddies and carry relatively large amounts of liquid mass (Chu and Dukler, 1975; Brauner and Moalem-Maron, 1983; Nosoko et al., 1996; Yoshimura et al., 1996), while the small waves are believed to enhance turbulent transport in the gas phase (Dukler, 1977). Since there are significant variations in the actual fraction of mass carried by the large-amplitude waves as reported by various researchers such as Dukler (1977), Nosoko et al. (1996) and Mudawar and Houpt (1993a), it is of interest to quantitatively examine the fraction of liquid mass carried by the waves based on the velocity profiles obtained in this work.

The instantaneous flow rate, Q_i, evaluated from the instantaneous mean velocity, normalized by the average liquid flow rate, Q_{ave}, is plotted against the normalized instantaneous liquid film thickness, δ/δ_{ave} in Fig. 13. Although the waves (regions of thick film) are seen to transport more liquid than regions of thin films, waves appear to carry less liquid than that predicted by Nusselt's (1916) theory for smooth films of the same thickness as the waves. This is consistent with the over-prediction of the time-averaged mean and maximum velocities by Nusselt's theory.

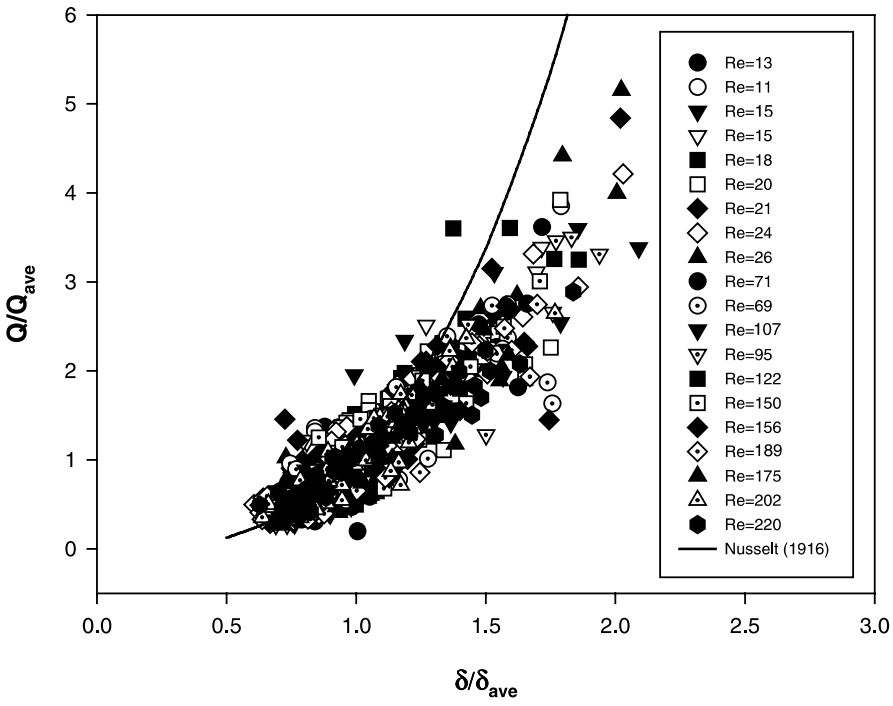

Fig. 13. Relationship between liquid mass transport and film thickness.

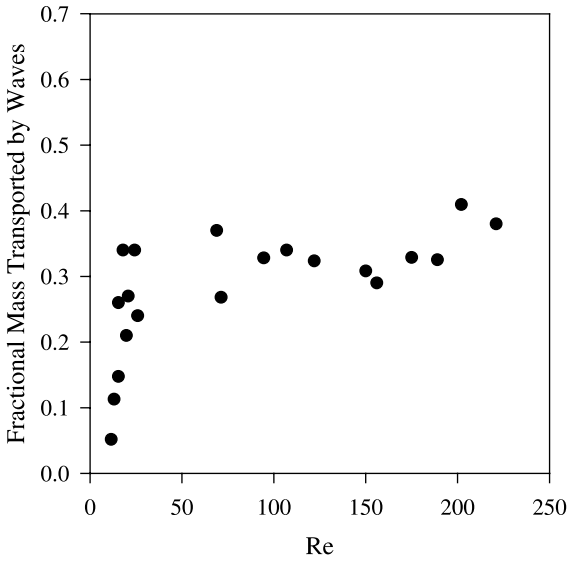

Fig. 14. Fraction of liquid mass transported by waves.

The instantaneous flow rates in waves and non-wave regions can be separately added to determine the fractions of liquid mass transported by the waves and substrate film. However, the mass flow rate can be evaluated in several different ways, which could yield significantly different results. In the first method used here as well as in other studies, only the liquid carried in layers beyond the substrate film thickness, which is given by the peak in the p.d.f. of the film thickness, is accounted for. This method revealed that the mass fraction of liquid carried by the waves increased from 12% to 35% of the total liquid mass at low Reynolds numbers, $11 < Re < 26$, and then reached 40–50% at higher Reynolds numbers, $69 < Re < 220$.

The second method was based on the entire liquid mass flowing between the wall and interface under the large waves, which were identified by examining the consecutive film thickness data and applying a criterion explained previously, $(\delta_{i-1} < \delta_i > \delta_{i+1})$ and $\delta_i > 1.15\delta_{\text{ave}}$. As shown in Fig. 14, this method yielded mass fractions ranging from less than 10% at the lowest Reynolds number of 11 to about 35% at $Re = 26$, and then reaching relatively constant values of 30–40% at larger Reynolds numbers up to $Re = 220$.

Literature values exhibit significant variations possibly due to differences in the fluid properties, definition of waves and method of mass flow rate evaluation under the waves. For water films ($\gamma \sim 3000$), Dukler (1977) estimated that more than 90% of mass was transported by waves in a falling film at $Re < 1000$, while Nosoko et al. (1996) gave estimates of 86–92% at $Re = 14$–90. In contrast, for more viscous fluids with small Kapitza numbers, smaller fractions similar to the present results have been reported previously. For a vertical film of water–90% propylene glycol solution, Mudawar and Houpt (1993a) reported that only 40% of the liquid mass was carried by large waves at $Re = 209$. Thus, the present values based on two different methods of calculation are consistent with the results of Mudawar and Houpt (1993a) for a viscous film with a small Kapitza number, rather than those of Dukler (1977) and Nosoko et al. (1996) for water films with

a large Kapitza number. These results may be attributed to the thickening of the substrate film with an increase in viscosity or reduction in the Kapitza number.

3.2.5. Wall shear stress and film thickness variations

The present results indicated a linear dependence of time-averaged wall shear stress on film thickness (Table 1), as suggested by Nusselt (1916), however, the instantaneous data indicated the constant of proportionality to be slightly different from that predicted by Nusselt (1916). In addition, a large degree of scatter was observed and the relationship was not as apparent as that for the flow rate (Fig. 13), or velocity (Fig. 4). Thus, the instantaneous wall shear stress normalized by the gravitational force per unit area, $\tau_w/\rho g\delta\cos\theta$, and instantaneous film thickness normalized by the time-averaged value, δ/δ_{ave}, were carefully compared as functions of time to further examine this dependence (Fig. 15). At low Reynolds numbers, the normalized wall shear stress and normalized film thickness were nearly equal and fluctuated with the passage of waves. As the Reynolds number increased, the deviations between the normalized wall shear stress and film thickness became more common. The largest deviations consistently occurred throughout all runs in the wave region, where the normalized wall shear stress, in most instances, did not achieve the same maximum values as the corresponding film thickness. As for the timing of peaking, the peaks in wall shear stress more often preceded the film thickness peaks than lagged behind or coincided with each other, as evident in Fig. 15. This is consistent with the results of both Miya et al. (1971) and Wasden and Dukler (1989) who reported that the wall shear stress peaks occur slightly ahead of the film thickness peaks for water ($\gamma \sim 3000$).

Finally, all of the instantaneous wall shear stress data collected were statistically analyzed in each of the four regions of a wavy film. The instantaneous values of $\tau_w/\rho g\delta\cos\theta$ were averaged in each region and are shown in Table 2. These results show that in the wave region, the wall shear stress is significantly less than the gravitational force per unit area, but the opposite applies to the substrate film. In the wave-front and wave-back regions, the values of $\tau_w/\rho g\delta\cos\theta$ are between those of wave and substrate regions, as expected.

From the point of view of a steady momentum balance, the above results suggest that the fluid accelerates in the wave ($\tau_w < \rho g\delta\cos\theta$), but decelerates in the substrate film, as $\tau_w > \rho g\delta\cos\theta$. Although the steady force balance would not strictly apply to a wavy film because convection terms must be included in the momentum equation, the present work strongly suggests a locally unsteady flow in the falling liquid film in which the fluid primarily accelerates in the large waves, slows down in the wave-back region and decelerates in the substrate film before accelerating again in the wave-front region.

The above results also support numerical predictions of wall shear stress variations in a vertically falling laminar film of water ($\gamma = 3371$) at $Re = 600$ reported by Yu et al. (1995), although their Kapitza number was much higher than in the present work. Using a refined boundary layer model, they predicted substantially smaller wall shear stress values, being less than 60% of the gravitational force per unit area, $\rho g\delta$, for two large waves with peak-to-substrate thickness ratios of 2.6 and 3.9. In the wave-front, wave-back and substrate film regions, the wall shear stress was predicted to be greater than $\rho g\delta$. A sharp drop was also predicted in the wall shear stress at the leading edge of the wave, but this could not be experimentally observed in the present work.

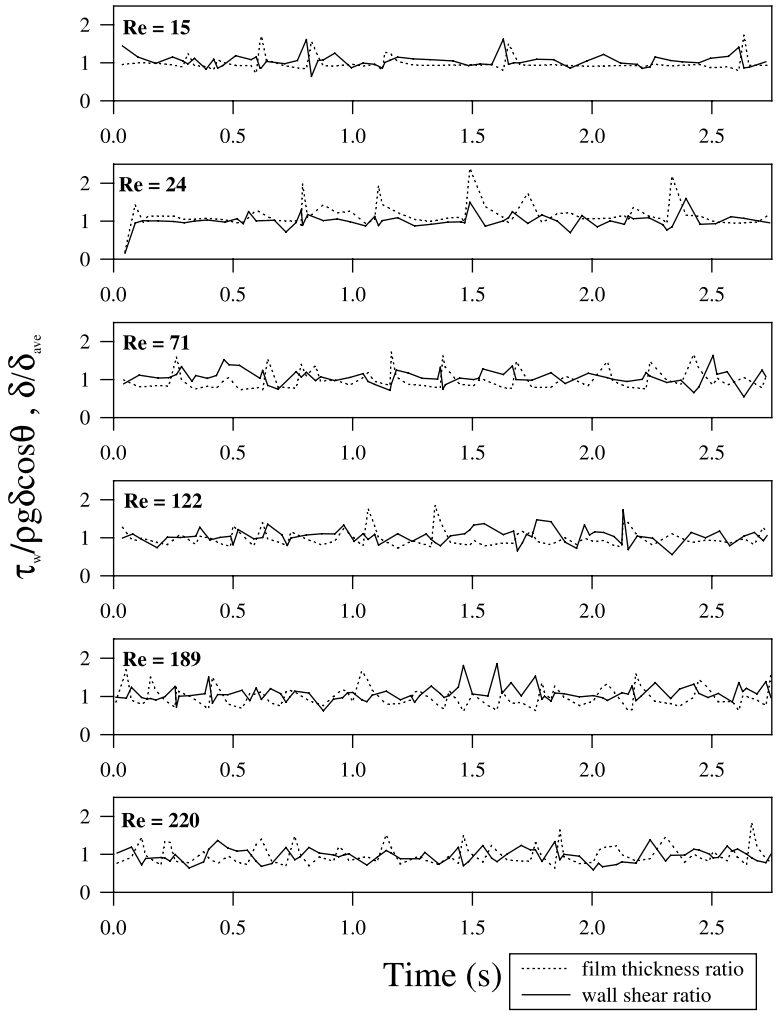

Fig. 15. Variations of instantaneous wall shear stress and film thickness with time.

4. Conclusions

Instantaneous measurements were performed, using a photochromic dye activation technique and high-speed video photography, to simultaneously determine the instantaneous film thickness, stream-wise velocity profile and wall shear stress for a wavy laminar liquid film of Kapitza number equal to 18.4 flowing over a flat plate with a 45° downward inclination. Experimental results indicated that the time-averaged film thickness data were slightly under-predicted by Nusselt's theory at Reynolds numbers between 11 and 220, while the mean velocity profiles were over-predicted by Nusselt's predictions for the same mean film thickness. Although the instantaneous velocity profiles were seen to generally conform to parabolic profiles in wavy laminar films, a strong influence of the waves was observed across the entire film thickness, even close to the wall.

The instantaneous velocity and wall shear stress data were also examined in different regions of the wavy laminar film. In the smooth film region, the instantaneous velocity profiles measured were close to Nusselt's predictions. However, under the waves, the velocity profiles were clearly over-predicted by Nusselt's theory on the average by 44%. Based on the measured velocity profiles, ~30–40% of liquid mass was seen to be transported by the large waves, consistent with a previous finding for a small Kapitza number fluid. The instantaneous wall shear stress data showed that in the substrate film, the values were close to the gravity force per unit area, but were smaller under the large waves. The temporal variations in wall shear stress and film thickness showed that the peaks in wall shear stress more often preceded the film thickness peaks, suggesting that the liquid in the wave region experiences acceleration while in the non-wavy region, both acceleration and deceleration are experienced.

Acknowledgements

This work was financially supported by a research grant and a graduate scholarship (for K.M.) from the Natural Sciences and Engineering Research Council of Canada.

References

Alekseenko, S.V., Nakoryakov, V.E., Pokusaev, B.G., 1985. Wave formation on vertical falling liquid films. Int. J. of Multiphase Flow 11, 607–627.

Alekseenko, S.V., Nakoryakov, V.E., Pokusaev, B.G., 1994. In: Fukano, T. (Ed.), Wave Flow of Liquid Films. Begell House, New York.

Aragaki, T., Toyama, S., Salah, H.M., Murase, K., Suzuki, M., 1990. Transition zone in a falling liquid film. International Chemical Engineering 30, 495–497.

Brauer, H., 1956. Stromung und warmeubergang bei reiselfilman. VDI-Forschungsheft, New York, p. 457.

Brauner, N., Moalem-Maron, D., 1982. Characteristics of inclined thin films, waviness and the associated mass transfer. Int. J. of Heat and Mass Transfer 25, 99–110.

Brauner, N., Moalem-Maron, D., 1983. Modeling of wavy flow in inclined thin films. Chem. Engin. Science 38, 775–788.

Chang, H.C., 1994. Wave evolution on a falling film. Annual Review Fluid Mechnics 26, 103–136.

Chang, H.C., Demekhin, E.A., Kopelevich, D.I., 1993. Nonlinear evolution of waves on a vertically falling film. Journal of Fluid Mechanics 250, 433–480.

Chu, K.J., Dukler, A.E., 1975. Statistical characteristics of thin, wavy films III: Structure of the large waves and their resistance to gas flow. AIChE Journal 21, 583–593.

Cook, R.A., Clark, R.H., 1971. The experimental determination of velocity profiles in smooth falling liquid films. Canadian Journal of Chemical Engineering 49, 412–416.

Dukler, A.E., 1977. The role of waves in two-phase flow: some new understandings. Chemical Engineering Educatation 11, 108–117.

Dukler, A.E., Bergelin, O.P., 1952. Characteristics of flow in falling films. Chemical Engineering Progress 48, 557–563.

Fulford, G.D., 1964. The flow of liquids in thin films. In: Advances in Chemical Engineering, vol. 5. Academic Press, NY, pp. 151–235.

Grimley, S.S., 1945. Liquid flow conditions in packed towers. Transactions Inst. Chem. Eng. 23, 228–235.

Ho, F.C.K., Hummel, R.L., 1970. Average velocity distributions within falling liquid films. Chem. Engin. Science 25, 1225–1237.

Jayanti, S., Hewitt, G.F., 1997. Hydrodynamics and heat transfer of wavy thin film flow. Int. J. of Heat and Mass Transfer 40, 179–190.

Kapitza, P.L., 1965. In: Ter-Haar, D. (Ed.), Collected Papers of Kapitza 1938–1964, vol. 2. Pergamon Press, NY, pp. 662–709.

Karapantsios, T.D., Paras, S.V., Karabelas, A.J., 1989. Statistical characteristics of free falling films at high Reynolds numbers. Int. J. of Multiphase Flow 15, 1–21.

Kawaji, M., 1998. Two-phase flow measurements using a photochromic dye activation technique. Nuclear Engineering and Design 184, 379–392.

Kawaji, M., Ahmad, W., DeJesus, J.M., Sutharshan, B., Lorencez, C., Ohja, M., 1993. Flow visualization of two-phase flows using photochromic dye activation method. Nuclear Engineering and Design 141, 343–355.

Koziol, K., Ulatowski, J., Franke, K., 1981. Velocity fields in falling films. International Chemical Engineering 21, 580–584.

Lyu, T.H., Mudawar, I., 1991. Statistical investigation of the relationship between interfacial waviness and sensible heat transfer to a falling liquid film. Int. J. of Heat and Mass Transfer 34, 1451–1464.

Miya, M., Woodmansee, D., Hanratty, T.J., 1971. A model for roll waves in gas–liquid flow. Chem. Engin. Science 26, 1915–1931.

Moalem-Maron, D., Brauner, N., Hewitt, G.F., 1989. Flow patterns in wavy thin films: numerical simulation. International Communications of Heat and Mass Transfer 16, 655–666.

Moran, K., 1997. An experimental study of laminar liquid films falling on an inclined plate. M.A.Sc. Thesis, Department of Chemical Engineering and Applied Chemistry, University of Toronto.

Mudawar, I., Houpt, R.A., 1993a. Measurement of mass and momentum transport in wavy-laminar falling liquid films. Int. J. of Heat and Mass Transfer 36, 4151–4162.

Mudawar, I., Houpt, R.A., 1993b. Mass and momentum transport in smooth falling liquid films laminarized at relatively high Reynolds numbers. Int. J. of Heat and Mass Transfer 36, 3437–3448.

Nagasaki, T., Hijikata, K., 1989. A numerical study of interfacial waves on a falling liquid film. ANS Proceedings National Heat Transfer Conference 4, 23–30.

Nakoryakov, V.E., Pokusaev, B.G., Alekseenko, S.V., Orlov, V.V., 1977. Instantaneous velocity profile in a wavy fluid film. Journal Engineering Physics 33, 1012–1016.

Nosoko, T., Yoshimura, P.N., Nagata, T., Oyakawa, K., 1996. Characteristics of two-dimensional waves on a falling liquid film. Chem. Engin. Science 51, 725–732.

Nusselt, W., 1916. Die oberflachenkondensation des wasserdamphes. VDI-Zs 60, 541.

Portalski, S., 1963. Studies of falling liquid film flow: film thickness on a smooth vertical plate. Chem. Engin. Science 18, 787–804.

Portalski, S., 1964. Eddy formation in film flow down a vertical plate. Industrial Engineering Chemical Fundamentals 3, 49–53.

Shkadov, V.Ya ., 1967. Wave conditions in the flow of thin layer of a viscous liquid under the action of gravity. Izv. Akad. Nauk SSSR Mekh. Zhidk. Gaza 1, 43–50.

Shkadov, V.Ya., Sisoev, G.M., 1999. Wavy falling liquid films: theory and computation instead of physical experiment. In: Proceedings of the IUTAM Symposium, Notre Dame University.

Stuhltrager, E., Miyara, A., Uehara, H., 1995. Flow dynamics and heat transfer of a condensate film on a vertical wall II: Flow dynamics and heat transfer. Int. J. of Heat and Mass Transfer 38, 2715–2722.

Takahama, H., Kato, S., 1980. Longitudinal flow characteristics of vertically falling liquid films without concurrent gas flow. Int. J. of Multiphase Flow 6, 203–215.

Wasden, F.K., Dukler, A.E., 1989. Numerical investigation of large wave interactions on free falling films. Int. J. of Multiphase Flow 15, 357–370.

Wasden, F.K., Dukler, A.E., 1992. An experimental study of mass transfer from a wall into a wavy falling film. Chem. Engin. Science 47, 4323–4331.

Wilkes, J.O., Nedderman, R.M., 1962. The measurement of velocities in thin films of liquid. Chem. Engin. Science 17, 177–187.

Yoshimura, P.N., Nosoko, T., Nagata, T., 1996. Enhancement of mass transfer into a falling laminar liquid film by two-dimensional surface waves—some experimental observations and modeling. Chem. Engin. Science 51, 1231–1240.

Yu, L.Q., Wasden, F.K., Dukler, A.E., Balakotaiah, V., 1995. Nonlinear evolution of waves on falling films at high Reynolds numbers. Physics of Fluids 7, 1886–1902.